UNIVERSITY OF
BATH

University of Bath

Error estimates for semi-Lagrangian finite difference methods applied to Burgers' equation in one dimension

Stephen Cook[a], Chris Budd[a,*], Adrian Hill[a], Thomas Melvin[b]

[a]*University of Bath, BA2 7AY, UK*
[b]*Met Office, FitzRoy Road, Exeter, EX1 3PB, UK*

Abstract

We make an analytic study of the diffusive,dispersive and overall errors, which arise when using semi-implicit semi-Lagrangian (**SISL**) finite difference methods to approximate those travelling wave solutions of the one-dimensional Burgers' equation with small diffusion, which develop sharp fronts. For the case of a fixed uniform spatial mesh, with piecewise linear interpolation, a backward error analysis approach is used to construct a precise formal analytic description of the front profile of the numerical approximation to this solution. From this description it is possible to obtain precise estimates of the front width and the front speed in terms of the spatial and temporal step size and to express the overall solution error in terms of these. These formal estimates agree closely with numerical calculations, both qualitatively and quantitatively, and display a roughly periodic behaviour as the number N_x of mesh points increases, and the CFL number passes through integer values. In particular, they show that despite the otherwise poor resolution of the method, that the front width is closely approximated when the CFL number is close to an integer, and the front speed is closely approximated when it is close to a half integer. The overall L_2 error also shows super-convergence for certain values of N_x. This possibly motivates doing two calculations with different N_x when using the SISL method on such problems to separately minimise the diffusive and dispersive errors. Similar errors in the front width and speed are observed for a number of different interpolation schemes with and without flux limiters.

Keywords: semi-implicit, semi-Lagrangian, Burgers' equation, error estimates, modified equation, numerical weather prediction

---

*Corresponding author

1. Introduction

1.1. Overview

The Semi-Implicit Semi-Lagrangian (SISL) algorithm is a popular method for numerical weather prediction. It is described in [SC91, Rob81, Rob82, CGM$^+$98, RTS$^+$95, WSW$^+$14] with theoretical error analysis presented in [FF98]. In this method (to be described in detail in Section 2) the solution is discretised over each time step Δt along a locally defined Lagrangian particle path. An implicit calculation of the solution and its derivatives is then made at each stage of the calculation. This procedure can overcome some of the issues associated with the CFL constraint. The ability to take long time steps stably, along with a high order of accuracy for the advective terms, has led to the SISL method being widely used for NWP, including the dynamical cores of models at the Met Office [WSW$^+$14], the European Centre for Medium-Range Weather Forecasts [THA01], the China Meteorological Administration [CXY$^+$08] and the Canadian Meteorological Centre [CGM$^+$98], among others. However, the use of SISL methods requires the calculation, at each time step, of the departure (or arrival) points of the semi-Lagrangian paths, and the interpolation of the solution described on the computational mesh, onto these new points. The calculation of these departure points, and the subsequent interpolation of the solution, leads to additional errors in the calculation of the solution. These errors, particularly those due to the interpolation error, are greatly exacerbated when the solution changes rapidly (as in the case of a front) over a small region in space and can be compounded when a small time step Δt is used, requiring more interpolation steps. A consequence of this is that a *reduction* in the temporal step size can actually result in an *increase* in the overall solution error. This was proved rigorously in [FF98] for a class of SISL methods applied the (linear) advection equation, and we see similar results here for the case of the nonlinear Burgers' equation with a sharp front.

1.2. Results

The purpose of this paper is to use the modified equation method (backward error) analysis to make a formal study of the diffusive, dispersive, and overall errors that arise when applying a fixed mesh finite difference SISL method, with N_x mesh points, fixed spatial step $\Delta x = L/N_x$ where L is the domain width, temporal step Δt, and various interpolation schemes, to approximate the travelling wave solutions of the one dimensional Burgers' equation. (The modified equation method derives a PDE which is a closer approximation to the solution of the numerical method than the original PDE. The behaviour of this modified equation is then studied in detail. See [HLW06], [LR05] for more details of this approach to error analysis.) This equation is given in non-dimensional units as

$$u_t + uu_x = \varepsilon u_{xx} \,, \qquad (1)$$

where subscripts denote the partial derivatives, with $\varepsilon \ll 1$ and

$$u(-\infty, t) = c + \alpha \,, \quad u(\infty, t) = c - \alpha, \quad \forall \quad t > 0 \,, \qquad (2)$$

for some constant α. Note that ε can be thought of as a viscosity parameter with units $m^2 s^{-1}$. Burgers' equation (1) is chosen as a prototypical nonlinear advection equation which is known (with suitable initial conditions) to develop travelling wave solutions of wave speed c with sharp fronts, in which the solution varies rapidly over a length scale of order $\mathcal{O}(\varepsilon/\alpha)$ with profile given by

$$u(x,t) = c - \alpha \tanh \left(\frac{\alpha(x - ct)}{2\varepsilon} \right). \tag{3}$$

We expect ε to be very small in applications, so that for any realistic numerical scheme we have

$$\Delta x/\varepsilon \gg 1.$$

The solution (3) will then be poorly resolved by the numerical method, and errors will arise in the application of the SISL method due to errors in the discretisation, location of the departure points, and interpolation of the solution onto these points. We will show that the combined effect of these errors means that, whilst the numerical method also admits a travelling wave solution of the tanh profile form given by (3), this solution has a diffusive error leading to a different front width, given by $\widehat{\varepsilon}/\alpha$ with

$$\varepsilon \ll \widehat{\varepsilon} = \mathcal{O}(\Delta x).$$

There is also a dispersive error giving a wave speed $\widehat{c}$ in (3), which can be both less than, or greater than, the true wave speed of c, depending upon Δx and Δt. In addition, if a non monotonic interpolation scheme is used, the solution will typically be oscillatory close to the front due to (classical) approximation errors. The combination of the diffusive, dispersive and interpolation/approximation errors then combine to give the overall solution error, in which it appears that the dominant contribution is the dispersive error.

Although the finite difference SISL method does not necessarily have a CFL stability constraint (indeed this is a key advantage to their use in practice), we see rather different, and *approximately periodic*, behaviour in the errors as the mean CFL number defined via the expression

$$\nu_{\text{CFL}} = c \frac{\Delta t}{\Delta x} = c \frac{t_{\max}}{N_t} \frac{N_x}{L},$$

passes through integer values with increasing N_x, and as a result the semi-Lagrangian paths cross over the mesh points. We illustrate this in Figure 1, in which we see the numerically calculated wave speed $\widehat{c}$ of the front of the solution of the equation (1) in the case of the true speed $c = 1$. Here we plot $\widehat{c}$ as a function of the number N_x of the spatial mesh points, with a fixed time step Δt.

We will show analytically, by studying the modified equation for the finite difference SISL scheme with *linear interpolation* and in the limit of small α, that if

$$\mathcal{N} \equiv \lfloor \nu_{\text{CFL}} \rfloor$$
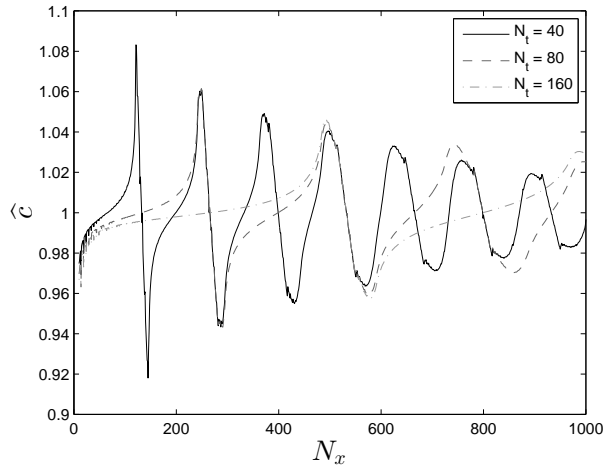
Figure 1: Numerically calculated values of the modified front speed $\widehat{c}$ as a function of the number of spatial mesh points N_x. This calculation finds an approximate solution of equation (1) taking $\alpha = 0.1$, $\varepsilon = 10^{-4}$ and $c = 1$. The figure is plotted for three values of the number of time steps N_t. In this case $\Delta x = 5/N_x$ and $\Delta t = 1.5/N_t$, so that that $\nu_{\mathrm{CFL}} = 0.3 N_x/N_t$. We see that $\widehat{c}$ oscillates either side of c. The jumps in $\widehat{c}$ arise when ν_{CFL} takes integer values, and we have $\widehat{c} = c$ (and the smallest error in the estimation of c) when ν_{CFL} takes half-integer values. Note also that the maximum error close to the integer ν_{CFL} values decreases slowly as N_x increases, and hence Δx decreases.

is the integer part of ν_{CFL} then, to leading order,

$$\widehat{\varepsilon} = \varepsilon + ((2\mathcal{N} + 1)\Delta x - c\Delta t)\frac{c}{2} - (\mathcal{N}^2 + \mathcal{N})\frac{\Delta x^2}{2\Delta t} + \mathcal{O}(\alpha(\Delta x^2 + \Delta t^2)). \quad (4)$$

A key observation from this result is that the error in the diffusion parameter can depend *inversely* on the time step Δt. A rough motivation for this apparantly counter-intuitive behaviour, is that the smaller the value of Δt, the more interpolation steps are required, each of which has an error proportional to Δx^2. A similar result for the case of the errors made in approximating the solutions of the linear advection equation, was proved rigorously in [FF98] (see equation (6.5) in that reference).

Similarly, for the same scheme and in the same limit of small α, we find the wave speed $\widehat{c}$ is to leading order given by the formal expression

$$\widehat{c} = c - \frac{\alpha^2}{6\widehat{\varepsilon}}\left((2\mathcal{N} + 1)\Delta x - 2c\Delta t\right) + \mathcal{O}(\alpha^2(\Delta x^2 + \Delta t^2)). \quad (5)$$

The resulting profile is then given by

$$\hat{u}(x,t) = c - \alpha \tanh\left(\frac{\alpha(x - \widehat{c}t)}{2\widehat{\varepsilon}}\right). \quad (6)$$

4

We will demonstrate, through numerical calculations presented in Figures 5 and 6, supported later by an analytic calculation, that when a monotonic interpolation scheme is used, the expression in in (6) is an excellent representation of the numerical solution. Hence the overall solution error E at a fixed time t is given by the estimate

$$E = \alpha \, \| \tanh(\alpha(x - ct)/\epsilon) - \tanh(\alpha(x - \widehat{c}t)/\widehat{\varepsilon}) \| \tag{7}$$

where $\| \bullet \|$ is any appropriate error norm. In Figure 15 we will also demonstrate that when a non monotonic interpolation scheme is used, the rescaled function in (6) gives a good representation of the front width and speed, upon which is superimposed an additional oscillatory approximation error arising from the interpolation scheme.

As an alternative presentation of the same formulae we fix the CFL number ν_{CFL} as

$$\nu_{\mathrm{CFL}} = \mathcal{N} + Y, \quad 0 \leq Y < 1,$$

and consider the limit as $\Delta x \to 0$ with $\Delta t = \nu_{\mathrm{CFL}} \Delta x / c$. It follows from (4) that

$$\widehat{\varepsilon} = \varepsilon + \frac{c \, Y(1 - Y) \, \Delta x}{2\nu_{\mathrm{CFL}}} + \mathcal{O}(\alpha \Delta x^2).$$

Similarly, on rescaling (5), the front speed is given by the expression

$$\widehat{c} = c - \frac{\alpha^2 \, (1 - 2Y) \, \nu_{\mathrm{CFL}}}{3cY(1 - Y) + 6\varepsilon\nu_{\mathrm{CFL}}/\Delta x} + \mathcal{O}(\alpha^2 \Delta x^2).$$

If $\Delta x \gg \varepsilon$ and we are away from integer values of ν_{CFL}, this expression simplifies to

$$\widehat{c} = c - \frac{\alpha^2 \nu_{\mathrm{CFL}} \, (1 - 2Y)}{3c \, Y(1 - Y)} + \mathcal{O}(\alpha^2 \Delta x^2), \tag{8}$$

and we see that, in the asymptotic limit, $\widehat{c}$ is almost independent of Δx until $\Delta x = \mathcal{O}(\varepsilon)$.

We see that $\widehat{\varepsilon}$ is smallest, and approaches the true value, when $Y \in \{0, 1\}$ despite the large step size and poor resolution of the method. This is to be expected as in this case the departure points of the semi-Lagrangian paths coincide with the mesh points, so there is minimal interpolation error. In contrast, the wave speed is exactly equal to the true speed c when $Y = 1/2$. This consistent with the numerical results presented in Figure 1. As ν_{CFL} passes through integer values and Y jumps from 1 to 0 we see a rapid change in the dispersive error $\widehat{c} - c$. If ν_{CFL} is just smaller than an integer then c is over estimated, and if ν_{CFL} is just bigger, then it is under estimated. The maximum value of the over/under estimate close to the integer value of ν_{CFL} is given to leading order by

$$|\widehat{c} - c| \sim \frac{\alpha^2 \Delta x}{6\varepsilon}. \tag{9}$$

This leads us to the conclusion that to fully resolve the solution we might wish to do two calculations for integer, and half-integer values of the CFL number.

In Figures 2 and 3 we present the numerically calculated values of $\widehat{\varepsilon}$ and $\widehat{c}$ for a variety of values of ν_{CFL}. These figures fully support the conclusions from the formulae (8) and (9).
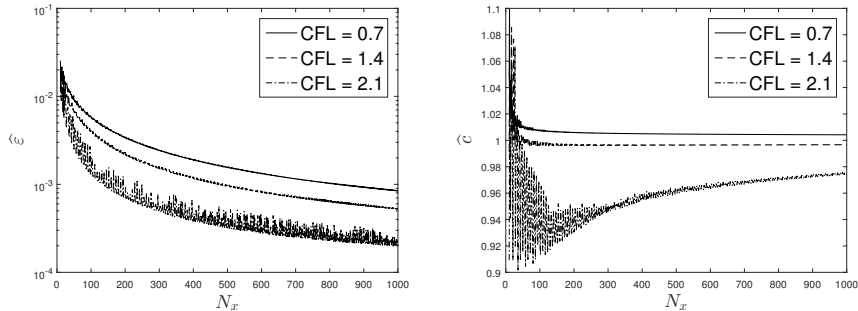
Figure 2: Numerically calculated values of the modified diffusion $\widehat{\varepsilon}$ and front speed $\widehat{c}$ as a function of the number of spatial mesh points N_x when the CFL number is fixed. Note that $\widehat{c}$ is independent of N_x for large N_x. We see from these figures that $\widehat{\varepsilon}$ is best approximated when ν_{CFL} is close to an integer, and $\widehat{c}$ when ν_{CFL} is close to a half integer.
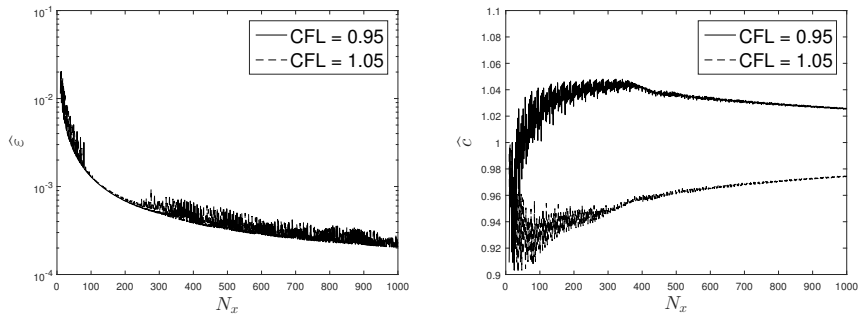
Figure 3: Numerically calculated values of the modified diffusion $\widehat{\varepsilon}$ and front speed $\widehat{c}$ as a function of the number of spatial mesh points N_x when ν_{CFL} is fixed at values just below, and just above, $\nu_{\mathrm{CFL}} = 1$. We see that $\widehat{\varepsilon}$ is well approximated in both cases (taking the same values) and that $\widehat{c}$ jumps either side of the correct value of $c = 1$.

Although these results are obtained by formal arguments only, assuming α to be small, they will be verified through a set of numerical experiments which give both good quantitative and qualitative agreement with these calculations. We will also repeat the numerical experiments for larger values of α and will again obtain good qualitative agreement. Furthermore, we will reproduce these calculations using a different set of interpolation procedures. Again we will see very similar qualitative behaviour of both the artificial diffusion parameter and

also the wave speed of the front, although the overall solution error includes a contribution from the oscillatory interpolation/approximation error. Plots of the modified diffusion and front speed for fixed CFL number with higher-order interpolants look similar to the case with a linear interpolant (Figures 2 and 3) and are not included.

1.3. Summary

The layout of the remainder of this paper is as follows: In Section 2 we describe the basic SISL method for one dimensional advective equations and briefly discuss some existing error analysis of these methods. In Section 3 we apply the SISL method to Burgers' equation (1) and, by using a formal modified equation analysis, show that it admits travelling wave solutions of the general form (3) with front width $\widehat{\varepsilon}$ given by (4); we also calculate the effective wave speed $\widehat{c}$, given by (5) and an estimate for the overall L_2 solution error. In Section 4 we analyse the results of the formal calculation and discuss their implication. In Section 5 we show the results of numerical calculations, which support these formal calculations. Finally in Section 6 we draw some conclusions from this work and consider future extensions of the methods used. In particular, as a dominant cause of the error is in the interpolation step we propose the use of a mesh adaption procedure to reduce the interpolation errors at each stage of the calculation.

2. Finite difference SISL Methods with a fixed spatial mesh

The SISL method is the combination of a semi-implicit (SI) time stepping scheme, to remove any stability constraints from fast waves, along with a semi-Lagrangian (SL) method to provide an accurate and stable representation of the advective terms. For a semi-implicit scheme, following [SC91], only the terms that correspond to fast but physically unimportant waves (such as acoustic waves in the atmosphere) are treated implicitly, so that the overall scheme is not restricted by any CFL condition on waves that carry little physical relevance. Within both parts of the SISL method there are a number of flavours, such as using two- or three-time-level schemes and the method chosen to compute the semi-Lagrangian trajectories. Here we will concentrate on the form of SISL used in the Met Office model [WSW^{+}14].

2.1. Overview

In this section, we will describe the popular *two time-level SISL* algorithm used to approximate the solution of a nonlinear advection dominated one-dimensional partial differential equation (PDE), which we assume has the form

$$\frac{Du}{Dt} = F\left(u, u_x, \varepsilon u_{xx}\right), \quad x \in [a, a + L], \quad t > 0, \quad \varepsilon \ll 1, \qquad (10)$$

7

where

$$\frac{D}{Dt} \equiv \frac{\partial}{\partial t} + u\frac{\partial}{\partial x}$$

is the advective derivative. The basic philosophy behind all semi-Lagrangian methods is to find approximations for the particle paths of the solutions of (10), and to then calculate an approximation to the advective derivative along these paths. Integrating (10) along a semi-Lagrangian trajectory, from the departure point X_D at t to the arrival point X_A at $t + \Delta t$ over a single time step, we obtain

$$u^{t+\Delta t}(X_A) - u^t(X_D) = \int_t^{t+\Delta t} F(u, u_x, \varepsilon u_{xx}) \, dt', \tag{11}$$

where subscripts A and D denote evaluation at arrival and departure points respectively. There are two main forms of semi-Lagrangian methods.

For a *forward semi-Lagrangian method* we depart from a given mesh at time t^n and calculate the arrival mesh at time level t^{n+1} from the advection; the fields are then interpolated back onto the given mesh for the next SL step. In this case, departure points are the known mesh points $X_{j,D} \equiv X_j$, and the solution at the arrival points has to be computed via interpolation.

We will adopt a different approach, and shall concentrate on the *backwards semi-Lagrangian method* which is widely used in the meteorological literature, for example in the ENDGame code [WSW$^+$14]. For this method, the arrival points $X_{j,A}$ are exactly the mesh points X_j at the time level t^{n+1}, and the departure points at the time level t^n are those points for which the Lagrangian paths starting at $X_{j,D}$ at time t^n arrive at $X_{j,A}$ at time t^{n+1}. Accordingly, let us assume that at time level $t^n = n\Delta t$ we have an approximate solution U_j^n given at all of the (fixed) mesh points

$$X_j = a + j\Delta x.$$

We then seek an approximation to the solution at time level t^{n+1}. In a Lagrangian method we find approximations to the particle paths which satisfy the equation

$$\frac{Dx}{Dt} = u \tag{12}$$

and discretise the solution along these. To complete the SISL discretisation, the right-hand side of (11) is approximated by

$$U^{n+1}(X_{j,A}) - U^n(X_{j,D}) = \Delta t \left[\theta F^{n+1}(X_{j,A}) + [1 - \theta] F^n(X_{j,D}) \right], \tag{13}$$

(where $0 < \theta \le 1$) and the dependencies of F have been dropped for convenience. The semi-implicit method will treat the terms that contribute to the fast waves in F^{n+1} implicitly, and the remaining terms are approximated in some way, such as extrapolation. If the fast wave contribution from F is $\mathcal{L}$ (and the remaining terms are $F - \mathcal{L}$) then (13) with a SISL discretisation becomes

$$\left[U^{n+1} - \theta \Delta t \mathcal{L}^{n+1} \right] (X_{j,A}) = \left[U^n + (1 - \theta) \Delta t F^n \right] (X_{j,D})$$
$$+ \theta \Delta t (F - \mathcal{L})^{n+1} (X_{j,A}).$$

Treating (12) in the same way yields

$$X_{j,A} - X_{j,D} = \Delta t \left[\theta_X \, U^{n+1} \left(X_{j,A} \right) + (1 - \theta_X) \, U^n \left(X_{j,D} \right) \right] , \qquad (14)$$

where $0 < \theta_X < 1$. For this paper we shall take $\theta = 1/2$ for all of the analysis; however, we will also consider some numerical calculations with $\theta > 1/2$. To complete the discretisation it remains to choose the method of interpolation from the solution at the mesh points onto the departure points of the Lagrangian paths, and to choose the spatial discretisation of the approximation.

It is now assumed that we will approximate the function $u(x,t)$ on a *fixed* spatial mesh $x \in [a, a + L]$, with N_x mesh points, so that the mesh size is $\Delta x = L/N_x$. If the time step is Δt then the approximation to $u(x,t)$ is given by

$$U_j^n \approx u(a + j\Delta x, n\Delta t) .$$

Following [WSW+14] the departure points $X_{j,D}$, according to (14), are calculated iteratively, with the $u^n \left(X_D \right)$ term lagged in the iterates. Observing the change in the departure points over these iterates, we see this process rapidly converges; we find 10 iterates to be sufficient to reach convergence for all time steps. The solution at time level t^n is then interpolated onto these departure points. As we shall see, both the calculation of these points and the interpolation of the solution onto these points can lead to (possibly large) errors. The choice of the underlying finite difference spatial discretisation, made in this paper, follows the ENDGame formulation using centred finite differences. However, in principle there is no barrier to using other forms of discretisation in the implementation of SISL methods, such as a spectral [THA01], [GPF03] or finite element Galerkin methods [GNQ14], [TB15]. In this paper we will restrict our error analysis to finite difference methods only, but we will give indications of how it could be extended to the finite element case.

Interpolation to the departure points For a positive CFL number the departure point $X_{j,D}$ lies between two mesh points so that

$$X_{j-\mathcal{N}-1}^n < X_{j,D} \leq X_{j-\mathcal{N}}^n$$

where $\mathcal{N}$ is the integer part of the CFL number. An important part of the semi-Lagrangian method is the interpolation step, where we project the solution onto the departure points. In operational codes, various methods of interpolation are used, most commonly some form of Lagrangian polynomials. The simplest of these is *linear interpolation*, so that

$$U_{j,D} = y U_{j-\mathcal{N}-1}^n + (1 - y) U_{j-\mathcal{N}}^n , \quad y = \frac{X_{j-\mathcal{N}}^n - X_{j,D}}{X_{j-\mathcal{N}}^n - X_{j-\mathcal{N}-1}^n} .$$

The analytical error estimates presented in Section 2 will assume that linear interpolation is used. In practice, higher order methods are often used instead. Of these, cubic-Lagrange interpolation is a popular choice, providing a good

9

balance between accuracy and computational cost. The cubic-Lagrange interpolant of a function $f(x)$ for an interval $[x_i, x_{i+1}]$ is the unique cubic which passes through points f_{i-1}, f_i, f_{i+1} and f_{i+2}, where $f_j = f(x_j)$. Alternatively, a number of other choices could be made, such as to use the essentially non-oscillatory (ENO) cubic interpolant [HEOC87], or weighted essentially non-oscillatory (WENO) interpolants [LOC94]; a cubic Hermite interpolant can be used which is uniquely determined on $[x_i, x_{i+1}]$ by the points f_i, f_{i+1} and the gradients d_i, d_{i+1}, where $d_j = f'(x_j)$ (determined numerically). A cubic Hermite interpolant can be guaranteed to be monotonic by ensuring the gradients sit within a specific range [FC80, dBS77]. Rasch and Williamson [RW90] compared a number of different interpolants and derivative estimates for semi-Lagrangian advection, and found some of the best all-round results with a monotonic cubic Hermite interpolant using a fourth-order finite difference estimate for the derivatives [Hym83].

2.2. The nature of the errors encountered when using finite difference SISL methods

The accuracy of the SISL algorithm has been studied by a number of authors: see for example [MM94, CK09, Smi00, McC88, McD84, McD87, FF98]. Of most relevance to the current paper is the observation in [McC88, McD84, McD87, FF98], that the interpolation step in the SISL introduces an error which takes the form of a dissipative change to the underlying solution. In these papers the dissipation factor for plane waves is calculated for a set of different interpolation strategies and fractions of the CFL number. In all cases a significant increase in the dissipation was observed, often inversely proportional to the time step Δt [FF98]. In this paper we will observe similar effects for nonlinear wave problems, and will extend the above analysis to a broader range of CFL numbers and also to look at the dispersive errors associated with the wave speed.

3. Error estimates in the application of the SISL method to Burgers' equation

In this section we give an error analysis of the SISL method with varying forms of interpolation, in the context of its application to the approximation of a travelling wave of speed c with a sharp gradient leading to a travelling front of narrow width ε. Such waves arise, for example, in Burgers' equation (1) with a small viscosity ε. In the context of this paper, Burgers' equation serves as a prototype of a more general class of nonlinear equations admitting waves with a sharp interface. The papers [Smi00, KW90, BS92] have considered semi-Lagrangian schemes applied to Burgers' equation and commented on the errors observed. We now make a systematic analysis of these errors. For monotonic interpolation schemes, for example piece-wise linear interpolation, these will manifest themselves in two ways: firstly a *dissipative* error, in which the width of the front is significantly over estimated; secondly a *dispersive* error, in which

the speed of the front is miscalculated. For non monotonic schemes there is a further error due to oscillations of the numerical solution close to the front. The overall error (7) is then a combination of these estimates. If the CFL is close to an integer the overall error is primarily dispersive. However if the CFL is close to a half integer, it is primarily diffusive.

3.1. Motivation

It is well known that Burgers' equation (1) with (2) has a stable family of travelling wave solutions of constant speed c which take the form (3). The most distinctive feature of this solution is the existence of the wave front which has width of order $\mathcal{O}(\varepsilon/\alpha)$ in which u has a large gradient

$$u_x(x^*, t) = -\frac{\alpha^2}{2\varepsilon} \tag{15}$$

at the centre of the front x^*. The wave is a prototype of frontal behaviour encountered in meteorology and of shock formation encountered in gas dynamics [LeV02]. When $\varepsilon/\alpha \ll 1$ such travelling waves are difficult to approximate using a fixed mesh numerical method. We now ask how well this behaviour is captured in the SISL scheme described in the previous section.

3.2. The SISL algorithm applied to Burgers' equation

Applying the SISL discretisation with $\theta = 1/2$ to Burgers' equation (1) gives the numerical scheme

$$\left(U_j - \frac{\Delta t}{2}\varepsilon\frac{[U_{j-1} - 2U_j + U_{j+1}]}{\Delta x^2}\right)_A^{n+1} = \left(U_j + \frac{\Delta t}{2}\varepsilon\frac{[U_{j-1} - 2U_j + U_{j+1}]}{\Delta x^2}\right)_D^n \tag{16}$$

along with the trajectory equation (14) with $\theta_X = 1/2$.

As the nonlinearity of Burgers' equation is tied up in the advective term and the only remaining term is the viscosity, which is treated in a centred implicit manner, (16) is the equivalent to a full centred semi-Lagrangian discretisation of Burgers' equation, i.e. there is no semi-implicit component in the definition of [SC91], that is an implicit treatment of only the fast wave terms. Nevertheless, viewing this as a prototype of what a SISL scheme would do with a more complicated model, we will, with a small abuse of notation, continue to describe this as a SISL discretisation.

We firstly perform an experiment in which $\varepsilon = 10^{-4}$, $\Delta x = 0.05$, $\Delta t = 0.0375$. We approximate the infinite spatial domain by the interval $[-1, 4]$ and take $u(-1, t) = 1 + \alpha$, $u(4, t) = 1 - \alpha$, $\alpha = 0.1$, so that the wave speed is $c = 1$, with $\nu_{\text{CFL}} = 0.75$, $\mathcal{N} = 0$. For this value of CFL we expect that the overall error will be an approximately equal combination of the diffusive and dispersive error terms. We use *linear interpolation* for all of our initial calculations, and apply the method given in Section 2 to find an approximate solution of Burgers' equation (1). The resulting x-profiles of $u(x, t)$ in the numerical

11
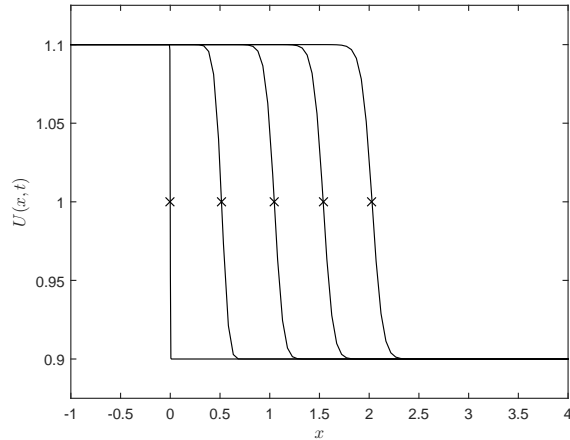
Figure 4: Initial condition and numerical solution to semi-Lagrangian Burgers' equation. Shown moving to the right are the initial condition at $t = 0$, and solutions at time steps 13, 27, 40 and 52, approximately corresponding to $t = 0.5$, 1, 1.5 and 2. The crosses correspond to the centres of the front x^* such that $U(x^*) = c = 1$.

experiment are given in Figure 4 for a series of values of increasing time t. A number of features are evident: firstly, it is clear that the application of the SISL scheme has led to a solution which takes the form of a travelling wave with a sharp front. To analyse this and subsequent numerical experiments, we introduce a number of measures. For each time t^n we find the centre of the front $x^{*,n}$ as the point where the linear interpolant of U_A^n equals c. To estimate the wave speed we denote the gradient of line of best fit to the curve $(t^n, x^{*,n})$ in the least squares sense as $\widehat{c}$. To estimate the effective viscosity parameter $\widehat{\varepsilon}$ we use finite differences to approximate the gradient u_x of the front over the interval containing x^* and at the final time. Then we use equation (15) to calculate the associated viscosity parameter from this gradient estimate. Accordingly, if $x^* \in [x_j, x_{j+1}]$, then we use the estimate

$$\widehat{\varepsilon} = -\frac{\alpha^2 \Delta x}{2\,|U_{j+1} - U_j|}\,. \tag{17}$$

We note at this stage (and we return to this calculation in more detail in Section 5) that the estimate for $\widehat{\varepsilon}$ above is limited by the discretisation. In particular, for the piecewise linear function U close to the front with $U_{j+1} - U_j < 2\alpha$, we have a lower bound for the numerical estimate of $\widehat{\varepsilon}$ given by

$$\varepsilon_{min} = \alpha \Delta x / 4\,. \tag{18}$$

The profile of the discrete travelling wave is closely approximated by a rescaling of the tanh-profile of the exact solution. To make this clearer we take $t = 1.5$ and in Figure 5 we compare the numerical solution U with the exact solution u (with

12

$c = 1$ and $\varepsilon = 10^{-4}$) in a vicinity of the front. A direct numerical calculation with the exact solution shows that mean square L_2 error $E = \|U - u\|_2$ at this time is given by $E = 1.893 \times 10^{-1}$. However, the figure is more revealing in that we can see that the numerical solution has a much broader front than the exact solution (a diffusive contribution to the error). Furthermore the centre of the front of the numerical solution at $x \approx 1.575$ is well in advance of that of the exact solution which is at $x = 1.5$ (a dispersive contribution to the error). To see how these two errors combine we compare the numerical solution U with a *rescaled travelling wave solution* $\hat{u}(x,t)$ of the tanh-profile form (6), again at the same time $t = 1.5$. In this case we take a modified diffusion and a modified speed given by $\hat{\varepsilon} = 0.00525$ and $\hat{c} = 1.05$. A direct numerical calculation shows that mean square L_2 error $\hat{E} = \|U - \hat{u}\|_2$ at this time is now given given by the much smaller value of $\hat{E} = 8.482 \times 10^{-3}$. As can be seen in Figure 5, the
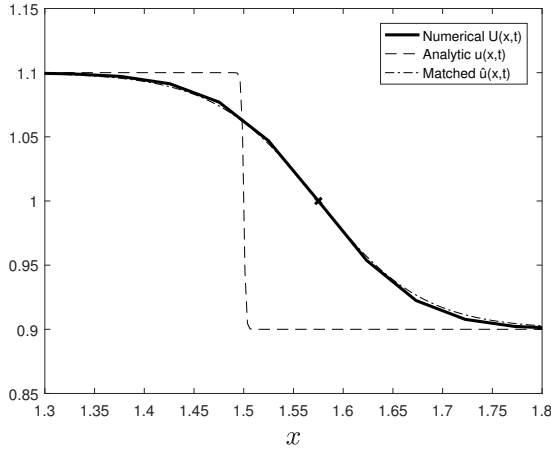
Figure 5: Comparison of the numerical solution with linear interpolation U (solid line), with the true solution u (dashed line) and the rescaled tanh-function $\hat{u}(x,t)$ (dash-dot line) at the time $t = 1.5$. In this figure it can be clearly seen that the front for the numerical solution is ahead of that of the analytical solution and is significantly broader. The rescaled tanh-profile $\hat{u}$ is almost indistinguishable from the numerical solution.

overall agreement between the numerical solution and the rescaled tanh-profile $\hat{u}(x,t)$ is very good. Indeed it is hard in the figure to tell one from the other for the whole of the window of x-values given. Further numerical experiments, not recorded here, confirm that the agreement between the solution of Burgers' equation using SISL and a rescaled tanh-profile is good for a wide variety of values of ε, N_x, N_t and times t^n. In all cases there is a significant deviation between the estimated front width $\hat{\varepsilon}$ and/or the speed $\hat{c}$, from the true values ε and c. We note that the computed values of $\hat{\varepsilon}$ and $\hat{c}$ above agree closely with the estimates in the formulae (4),(5).

For comparison we now perform the same experiment but this time use a mono-

13

tone cubic-Hermite interpolation scheme with a limiter to determine U at the departure points, as described in [Hym83]. The results of a computation of the front at $t = 1.5$ are presented in Figure 6. We can see again that the front is still broader than the true solution, although not quite as broad as that given by the linear interpolation scheme. There is also a significant dispersive error and the front is again ahead of that of the true solution. As in the case of the piecewise linear interpolation we can estimate the corresponding parameters $\widehat{\varepsilon}$ and $\widehat{c}$ to be $\widehat{\varepsilon} = 0.002136, \quad \widehat{c} = 1.0646$. Note that in comparison to the linear interpolant, this monotone interpolant leads to a numerical solution which has a smaller diffusive error (i.e. $\widehat{\varepsilon}$ is smaller) but a similar dispersive error. We also show in the figure a comparison of the rescaled tanh-profile $\hat{u}(x, 1.5)$ with these values. We see again that it is very close to the numerical solution. The corresponding L_2 errors are given by $\|U - u(x, 1.5)\|_2 = 2.5344 \times 10^{-1}$ and $\|U - \hat{u}(x, 1.5)\|_2 = 1.0879 \times 10^{-2}$.
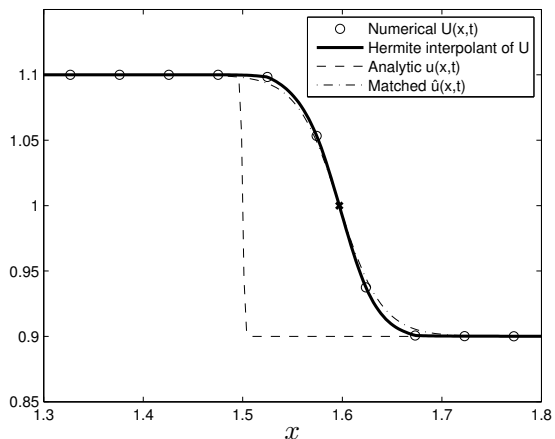
Figure 6: Comparison of the numerical solution with a monotone cubic-Hermite interpolation with a limiter U (solid line), with the true solution u (dashed line) and the rescaled tanh-function $\hat{u}(x, t)$ (dash-dot line) at the time $t = 1.5$. In this figure it can again be clearly seen that the front for the numerical solution is ahead of that of the analytical solution and is significantly broader. The rescaled tanh-profile $\hat{u}$ is again almost indistinguishable from the numerical solution.

3.3. Analysis of the errors arising when using SISL with linear interpolation

We now establish the formulae (4),(5) using a formal asymptotic argument.

3.3.1. Formal modified equation analysis

To perform the analysis of the errors, we firstly consider the errors of a semi-discrete (discrete in t) SISL discretisation of Burgers' equation taking the form

$$U_A^{n+1} - \frac{\Delta t \varepsilon}{2}(U_{xx})_A^{n+1} = U_D^n + \frac{\Delta t \varepsilon}{2}(U_{xx})_D^n , \qquad (19)$$

$$X_D = X_A - \frac{\Delta t}{2}\left[U_A^{n+1} + U_D^n\right] . \qquad (20)$$

For this first analysis we will assume that the term u_{xx} has *no discretisation error*. We consider the full discretisation error later, where we will show that the bulk of the error in the SISL calculation arises from the calculation of the location of the points X_D and of the interpolation of the solution onto these points. This observation also implies that the error analysis we have presented here for a finite difference (in space) discretisation will also apply to the case of a finite element discretisation of the same order of local accuracy. Indeed, for a general order scheme, equation (16) can be rewritten as

$$\left(M + \frac{\Delta t \varepsilon}{2}G\right)U_A^{n+1} = \left(M - \frac{\Delta t \varepsilon}{2}G\right)U_D^n, \qquad (21)$$

with mass matrix M (which is the identity for the finite-difference scheme considered here) and diffusion operator G. The analysis the follows as below with the following modifications: Contributions from M and the accuracy of G have to be taken into account in the discretisation, although typically as stated the interpolation error will dominate these. The expansion of U_D^n will be modified depending upon the interpolation operator used by the scheme. The expansion of U_D^n would then further be modified by the order of accuracy of the discrete mass matrix M and diffusion operator G. All of these considerations will then lead to a different modified equation in terms of V from which the analysis proceeds along similar lines to the finite difference example considered here.

For simplicity we give an analysis for the case of linear interpolation, but will present numerical calculations with different interpolation schemes later. Motivated by the results of the previous sub-section, we perform a backward error analysis by constructing the modified equation satisfied by an exact travelling wave solution to this scheme. Accordingly, let us assume that the SISL discretisation admits an exact travelling wave solution $U(x,t) = V(x - \widehat{c}\, t)$ with speed $\widehat{c}$, so that for all X_j and t^n the discrete solution $U_j^n \approx u(X_j, t^n)$ of the SISL scheme can be expressed as

$$U_j^n = V(X_j - \widehat{c}\, t^n) = V(z_j^n) \quad \text{where} \quad z_j^n = X_j - \widehat{c}\, t^n .$$

Our analysis will proceed by determining the leading order equation satisfied by the function $V(z)$, and solving this to give the shape of the wave and also its speed $\widehat{c}$. This will be achieved by considering a Taylor expansion of the travelling wave solution at the time t^{n+1} relative to the solution at time t^n. Accordingly, let $X_A = X_j$ be the arrival point. The solution at the arrival point

15
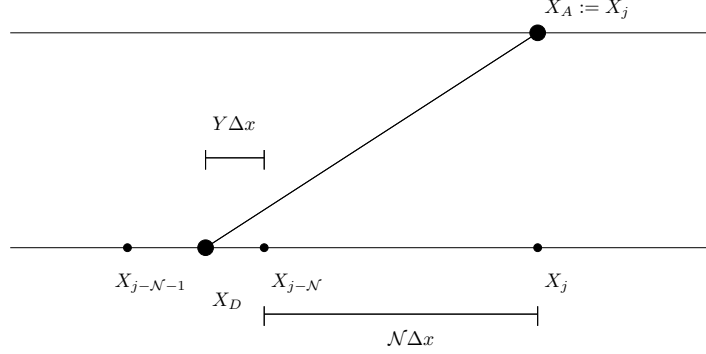
Figure 7: Demonstration of a typical trajectory showing $X_A - X_D = (\mathcal{N} + Y)\Delta x$.

(X_A, t^{n+1}) can then be considered to be a perturbation of the solution at the earlier time t^n via

$$U_A^{n+1} = V(X_j - \widehat{c}\, t^{n+1}) = V(X_j - \widehat{c}\, t^n - \widehat{c}\, \Delta t)$$
$$= V - \widehat{c}\, \Delta t V' + \frac{(\widehat{c}\, \Delta t)^2}{2} V'' + \mathcal{O}(\Delta t^3)\,.$$

Here the derivatives of $V(z)$ on the right-hand side are all evaluated at the point $z = z_j^n$. Similarly,

$$(U_{xx})_A^{n+1} = V'' - \widehat{c}\, \Delta t V''' + \mathcal{O}(\Delta t^2)\,,$$

and

$$U_A^{n+1} - \frac{\Delta t \varepsilon}{2}(U_{xx})_A^{n+1} = V + \Delta t \left(-\widehat{c} V' - \frac{\varepsilon}{2} V'' \right)$$
$$+ \frac{\Delta t^2}{2} \left(\widehat{c}^2 V'' + \widehat{c}\, \varepsilon V''' \right) + \mathcal{O}(\Delta t^3)\,. \quad (22)$$

We now determine the location of the departure points X_D. The location of these depends crucially on the CFL number $\nu_{\mathrm{CFL}} = c\Delta t/\Delta x$. For a single trajectory we shall call the floor of the number of grid-points spanned between the departure and arrival points $\mathcal{N}$, and the fractional part $Y = \nu_{\mathrm{CFL}} - \mathcal{N}$, such that $\mathcal{N} \in \mathbb{N}, \quad Y \in [0, 1)$, as demonstrated in Figure 7. From equation (20) we have

$$(\mathcal{N} + Y)\Delta x = X_A - X_D$$
$$= \frac{\Delta t}{2} \left(U_A^{n+1} + U_D^n \right)\,. \quad (23)$$

We note that if the CFL number is less than one, then $\mathcal{N} = 0$. However, $\mathcal{N}$ can also take values greater than zero. Taking the arrival point to be $X_A = X_j$, the

16

departure point X_D^n then lies in the interval $[X_{j-\mathcal{N}-1}, X_{j-\mathcal{N}}]$. We calculate the value of U_D^n at this point by using *linear interpolation*. In this case, we have

$$
\begin{aligned}
U_D^n &= I[U](X_D) \\
&= (1 - Y)U^n(X_{j-\mathcal{N}}) + Y\, U^n(X_{j-\mathcal{N}-1}) \\
&= \left(\frac{X_D - X_{j-\mathcal{N}-1}}{X_{j-\mathcal{N}} - X_{j-\mathcal{N}-1}} \right) U^n(X_{j-\mathcal{N}}) + \left(\frac{X_{j-\mathcal{N}} - X_D}{X_{j-\mathcal{N}} - X_{j-\mathcal{N}-1}} \right) U^n(X_{j-\mathcal{N}-1}).
\end{aligned}
\tag{24}
$$

The error made when interpolating a general twice differentiable function $f(x)$ over the interval $[X_{j-\mathcal{N}-1}, X_{j-\mathcal{N}}]$ (assumed of width Δx small) by a linear function $f_I(x)$ is well known [Pow81], and is given to leading order by

$$
f(x) - f_I(x) = \frac{1}{2}(x - X_{j-\mathcal{N}-1})(x - X_{j-\mathcal{N}})f_{xx}(x'),
$$

for some $x' \in [X_{j-\mathcal{N}-1}, X_{j-\mathcal{N}}]$. Taking the Taylor expansion of the travelling wave solution about X_j, we then have

$$
\begin{aligned}
U^n(X_{j-\mathcal{N}}) &= U^n\left(X_j - \mathcal{N}\Delta x\right) \\
&= V(z_j^n) - \mathcal{N}\Delta x V' + \frac{(\mathcal{N}\Delta x)^2}{2}V'' + \mathcal{O}(\Delta x^3), \\
U^n(X_{j-\mathcal{N}-1}) &= V(z_j^n) - (\mathcal{N}+1)\Delta x V' + \frac{((\mathcal{N}+1)\Delta x)^2}{2}V'' + \mathcal{O}(\Delta x^3).
\end{aligned}
$$

We now comment on the size of the errors in this expression and its resulting validity. The error in the interpolation and Taylor series expansion is dominated by terms of $\mathcal{O}(\Delta x^3 V''')$. In contrast, the smallest term in the expression, not considered in the error term, is given by $\Delta x^2 V''$. The error term is thus small compared with the previous terms, provided that

$$
\Delta x^3\, V''' \ll \Delta x^2\, V''
$$

which follows provided that

$$
\Delta x\, V'''/V'' \ll 1.
$$

Now, we will show, the solution to the modified equation (without the error term included) is given by the travelling wave of the form (6). A simple calculation shows that for such a travelling wave solution we have

$$
V'''/V'' = \mathcal{O}(\alpha/\widehat{\varepsilon}) = \mathcal{O}(\alpha/\Delta x).
$$

Here we have used the result (to be established later) that when we solve the modified equation we have

$$
\widehat{\varepsilon} = \mathcal{O}(\Delta x).
$$

17

It follows from this calculation that

$$\Delta x \, V'''/V'' = \mathcal{O}(\alpha).$$

Hence this expression is small, and the error terms in the modified equation are small, provided that

$$\alpha \ll 1. \tag{25}$$

The condition (25) will be essential in all of our future analysis.

Putting the terms above into equation (24) and rearranging gives

$$U_D^n = V - (\mathcal{N} + Y)\Delta x V' + \left((\mathcal{N} + Y)^2 + (1 - Y)Y\right)\frac{\Delta x^2}{2}V'' + \mathcal{O}(\Delta x^3). \tag{26}$$

We now combine this expression with the departure point equation in (23). This gives the expression

$$(\mathcal{N} + Y)\Delta x = \frac{\Delta t}{2}\left(V - \widehat{c}\,\Delta t V' + V - (\mathcal{N} + Y)\Delta x V'\right) + \mathcal{O}((\Delta x + \Delta t)^3).$$

We can rearrange this to get an explicit second order expression

$$(\mathcal{N} + Y)\Delta x = \Delta t\left(V - \frac{V + \widehat{c}}{2}\Delta t V'\right) + \mathcal{O}((\Delta x + \Delta t)^3). \tag{27}$$

We can substitute this into the interpolated departure point formula (26) to give the estimate

$$U_D^n = V - \Delta t V \, V' + \frac{\Delta t^2}{2}\left((\widehat{c} + V) \, V'^2 + V^2 \, V''\right)$$
$$+ \frac{\Delta x^2}{2}(1 - Y)YV'' + \mathcal{O}((\Delta x + \Delta t)^3).$$

We can now perform a similar analysis to evaluate the second derivative at the departure point $(U_{xx})_D^n$:

$$(U_{xx})_D^n = V'' - \Delta t V \, V''' + \mathcal{O}((\Delta x + \Delta t)^2). \tag{28}$$

Accordingly, we express the right-hand side of (19) as

$$U_D^n + \frac{\Delta t \varepsilon}{2}(U_{xx})_D^n = V - \Delta t\left(VV' - \frac{\varepsilon}{2}V''\right)$$
$$+ \frac{\Delta t^2}{2}\left((\widehat{c} + V) \, V'^2 + V^2 \, V'' - \varepsilon V \, V'''\right) + \frac{\Delta x^2}{2}(1 - Y)Y \, V''$$
$$+ \mathcal{O}((\Delta t + \Delta x)^3). \tag{29}$$

18

Substituting the expansions from equations (22) and (29) into the SISL discretisation (19) and rearranging leads to the following modified equation for $V(z)$:

$$\Delta t \left((V - \widehat{c})V' - \varepsilon V''\right) = \frac{\Delta t^2}{2} \left((\widehat{c} + V)V'^2 + \left(V^2 - \widehat{c}^2\right)V'' - (\widehat{c} + V)\varepsilon V'''\right)$$
$$+ \frac{\Delta x^2}{2}(1 - Y)Y\ V'' + \mathcal{O}((\Delta t + \Delta x)^3). \quad (30)$$

Finally, using the approximation for the location of the departure point (27), we can express the linear interpolation term in (30) as

$$\frac{\Delta x^2}{2}(1 - Y)Y\ V'' = \left(((2\mathcal{N} + 1)\Delta x - V\Delta t)\ V\Delta t - (\mathcal{N}^2 + \mathcal{N})\Delta x^2\right)\frac{V''}{2}.$$

Combining all of these results gives the following differential equation for V:

$$\Delta t \left((V - \widehat{c})\ V' - \varepsilon V''\right) = \frac{\Delta t^2}{2}(\widehat{c} + V)\left(V'^2 + (V - \widehat{c})\ V'' - \varepsilon V'''\right)$$
$$+ \frac{1}{2}\left[((2\mathcal{N} + 1)\ \Delta x - V\Delta t)\ V\Delta t - \left(\mathcal{N}^2 + \mathcal{N}\right)\Delta x^2\right]V''$$
$$+ \mathcal{O}\left((\Delta x + \Delta t)^3\right). \quad (31)$$

Full discretisation At this stage, we consider the additional error which arises when discretising the function εu_{xx} in (19), and hence of V'', in (31). Using the centred finite difference scheme $\delta^2 u$ with a uniform mesh, as in the expression (16), we have, from the well-known results on finite difference approximations, that

$$\varepsilon \frac{\delta^2 u}{\Delta x^2} = \varepsilon u_{xx} + \mathcal{O}(\varepsilon \Delta x^2 u_{xxxx}).$$

Hence, the error in approximating the $\Delta t \varepsilon V''$ expression in equation (28) by the centred difference $\Delta t \varepsilon \delta^2 V / \Delta x^2$ is of order $E_1 = \mathcal{O}\left(\varepsilon \Delta t \Delta x^2 V''''\right)$. Comparing with the error term $E_2 = \mathcal{O}(\Delta x^3 V''')$ we have, from the previous analysis, that $E_1/E_2 = \mathcal{O}(\varepsilon \alpha / \Delta x)$. Thus E_1 is much smaller than E_2 in the cases considered where α is small and $\varepsilon \ll \Delta x$. A similar estimate will also arise when a finite element scheme is implemented.

3.3.2. Heteroclinic solutions of the modified equation
We now consider the modified equation (31), and assume for the present that the terms of order $\Delta t^3, \Delta x^3$ and $\varepsilon \Delta x^2$ are small in comparison with the other error terms, and that Δx and Δt are of similar size. We observe that this is a nonlinear equation which is challenging to analyse in general. To study it, we will first identify the nature of the solutions we are interested in, then develop

19

an asymptotic series for these. To leading order we have

$$(V - \widehat{c}) \, V' = \varepsilon V'' + \frac{\Delta t}{2}(\widehat{c} + V)(V'^2 + (V - \widehat{c})V'' - \varepsilon V''')$$

$$+ \left(((2\mathcal{N} + 1)\Delta x - V\Delta t) \, V - (\mathcal{N}^2 + \mathcal{N})\frac{\Delta x^2}{\Delta t} \right) \frac{V''}{2}. \quad (32)$$

In the original system we have $u(\mp\infty, t) = c \pm \alpha$. It follows that the function $V(z)$ satisfies the asymptotic boundary conditions

$$V(-\infty) = c + \alpha, \quad V(\infty) = c - \alpha. \quad (33)$$

We now seek a solution to (32)–(33) which resembles the travelling wave solution to Burgers' equation. Suppose that this latter solution takes the form of a travelling wave of the form

$$u(x, t) = v(x - kt),$$

for some (unknown) speed k. The function $v(z)$ then satisfies the ordinary differential equation

$$(v - k) \, v' = \varepsilon v'' \quad (34)$$

with the same boundary conditions (33) as the modified equation. The two equations (32) and (34) are very similar. The most obvious difference between them is that the modified equation (32) has a more complicated right hand side.

The key qualitative feature of the travelling wave solution of the original equation (34) is that it has a solution which is a heteroclinic connection between the boundary conditions at $\pm\infty$, so that

$$v(z) \to c \pm \alpha \quad v'(z) \to 0, \quad \text{as} \quad |z| \to \infty.$$

We claim that this heteroclinic solution arises *only when* the wave-speed k is equal to c. This is a well known result [Dre83] which we summarise here. Integrating (34), and using the left asymptotic boundary condition that $v(-\infty) = c + \alpha$ and $v'(-\infty) = 0$, we have

$$\frac{v^2}{2} - kv = \varepsilon v' + \frac{(c + \alpha)^2}{2} - k(c + \alpha).$$

It then follows, that as $x \to \infty$ we must have

$$\frac{(c - \alpha)^2}{2} - k(c - \alpha) = \frac{(c + \alpha)^2}{2} - k(c + \alpha).$$

It follows from this identity that the wave speed of the original equation is uniquely given by

$$k = c.$$

We now claim that the modified equation (32) also has a solution $V(z) \approx v(z)$, which is also a heteroclinic connection (and hence is a travelling wave). Extending the form of the analysis given above, we will show that the condition for such a heteroclinic solution to exist, uniquely defines the wave speed $\widehat{c}$ of the modified solution.

3.3.3. Asymptotic analysis of the modified equation

To substantiate this claim, we consider an asymptotic analysis of a rescaled form of the modified equation in the limit of small α, developing an asymptotic series for the solution in powers of α. This gives a very useful way of systematically identifying the different contributions to the error. The revised diffusion value, solution profile and related front width are then given by considering terms in the asymptotic series of order $\mathcal{O}(\alpha^3)$, and the speed by considering terms of order $\mathcal{O}(\alpha^3)$ and $\mathcal{O}(\alpha^4)$. Whilst strictly only valid in the limit of $\alpha \to 0$, we find that the solution we obtain has excellent *quantitative* agreement with the numerical calculations when $\alpha = 0.1$. Also it gives useful *qualitative* information about the behaviour of the speed and front width for rather larger values of α. To perform this calculation, we are motivated by the scaling in α of the travelling wave solution (3) to the exact Burgers' equation. Accordingly, we introduce a rescaled function $W(s)$ through the transformation

$$V(z) = c + \alpha W(\alpha z), \quad s = \alpha z.$$

Under this rescaling, the leading order form of the modified equation becomes

$$
\begin{aligned}
\Delta t \left(\alpha^2 \left(c - \widehat{c} + \alpha W \right) W' - \alpha^3 \varepsilon W'' \right) \\
= \frac{\Delta t^2}{2} \left(c + \widehat{c} + \alpha W \right) \left(\alpha^4 W'^2 + \alpha^3 \left(c - \widehat{c} + \alpha W \right) W'' - \alpha^4 \varepsilon W''' \right) \\
+ \frac{\alpha^3 \Delta t}{2} \left[\left((2\mathcal{N} + 1) \Delta x - (c + \alpha W) \Delta t \right) (c + \alpha W) - \left(\mathcal{N}^2 + \mathcal{N} \right) \frac{\Delta x^2}{\Delta t} \right] W'' ,
\end{aligned}
$$

(35)

with asymptotic boundary conditions

$$W(-\infty) = 1, \quad W(\infty) = -1.$$

Here a prime now represents a derivative with regards to the rescaled variable s. We investigate this rescaled modified equation by formally expanding $\widehat{c}$ and $W(s)$ in terms of α so that

$$\widehat{c} = \widehat{c}_0 + \alpha \widehat{c}_1 + \alpha^2 \widehat{c}_2 + \cdots ,$$

(36)

$$W(s) = W_0(s) + \alpha W_1(s) + \alpha^2 W_2(s) + \cdots .$$

(37)

The boundary conditions of the modified equation

$$\lim_{z \to \mp\infty} V(z) = c \pm \alpha ,$$

give boundary conditions for the terms of the expansion as

$$
\begin{aligned}
\lim_{s \to \mp\infty} W_0(s) &= \pm 1 , \\
\lim_{s \to \mp\infty} W_i(s) &= 0 , \quad \text{for } i > 0 .
\end{aligned}
$$

(38)

21

In searching for a heteroclinic solution, as with the exact solution, we also observe that all derivatives of $W_i(s)$ tend to zero as s tends to $\pm\infty$ for all $i = 0, 1, \ldots$.

Substituting the formal expansions (36) and (37) into equation (35), we can consider terms in successive powers of α.

Terms of $\mathcal{O}(\alpha^2)$. Considering terms of order $\mathcal{O}(\alpha^2)$, we have

$$\alpha^2 \Delta t (c - \widehat{c}_0) W_0'(s) = 0 \,.$$

For non-trivial solutions in $W_0(s)$, we have

$$\widehat{c}_0 = c \,.$$

Terms of $\mathcal{O}(\alpha^3)$. Considering terms of order $\mathcal{O}(\alpha^3)$, we see that

$$\alpha^3 \Delta t \left((W_0 - \widehat{c}_1) W_0' - \widehat{\varepsilon} W_0'' \right) = 0 \,, \tag{39}$$

where

$$\widehat{\varepsilon} \equiv \varepsilon + \frac{1}{2} \left(((2\mathcal{N} + 1)\Delta x - c\Delta t) \, c - (\mathcal{N}^2 + \mathcal{N}) \frac{\Delta x^2}{\Delta t} \right) \,. \tag{40}$$

Integrating equation (39) over $[-\infty, \infty]$ gives

$$\left[\frac{W_0(s)^2}{2} - \widehat{c}_1 W_0(s) - \widehat{\varepsilon} W_0'(s) \right]_{-\infty}^{\infty} = 0 \,.$$

Substituting in the boundary conditions (38) gives

$$\widehat{c}_1 = 0 \,.$$

The equation (39) with $\widehat{c}_1 = 0$, together with the boundary conditions (38) has the well known heteroclinic solution

$$W_0(s) = -\tanh\left(\frac{s}{2\widehat{\varepsilon}} \right) \,, \tag{41}$$

(which without loss of generality we have centred on the point $s = 0$). This gives the numerical solution $V(z)$, to leading order of α

$$V(z) = c - \alpha \tanh\left(\frac{\alpha z}{2\widehat{\varepsilon}} \right) + \mathcal{O}(\alpha^2) \,,$$

Hence we see from this that to leading order the travelling wave has exactly the rescaled tanh-profile seen in Figure 5, with the numerical solution given by (6).

Terms of $\mathcal{O}(\alpha^4)$. To this order we have

$$\begin{aligned}
\alpha^4 \Delta t \left((W_1 - \widehat{c}_2) W_0' + W_0 W_1' - \widehat{\varepsilon} W_1'' \right) \\
= \alpha^4 \Delta t^2 c \left((W_0')^2 + W_0 W_0'' - \varepsilon W_0''' \right) \\
+ \alpha^4 \frac{\Delta t}{2} \left((2\mathcal{N} + 1)\Delta x - 2c\Delta t \right) W_0 W_0'' \,. \tag{42}
\end{aligned}$$

22

Integrating this equation over $[-\infty, \infty]$ leads to the expression

$$[-\widehat{c}_2 W_0(s) + W_1(s)W_0(s) - \widehat{\varepsilon}W_1'(s)]_{-\infty}^{\infty}$$
$$= \Delta t c \left[W_0(s)W_0'(s) - \varepsilon W_0''(s) \right]_{-\infty}^{\infty}$$
$$+ \frac{1}{2}((2\mathcal{N}+1)\Delta x - 2c\Delta t) \int_{-\infty}^{\infty} W_0(s)W_0''(s)\mathrm{d}s.$$

We can explicitly evaluate the integral using the solution from (41). Using this result and rearranging gives

$$\widehat{c}_2 = -\frac{1}{6\widehat{\varepsilon}}((2\mathcal{N}+1)\Delta x - 2c\Delta t).$$

Hence, combining results we have an expression for the front speed $\widehat{c}$

$$\widehat{c} = c - \frac{\alpha^2}{6\widehat{\varepsilon}}((2\mathcal{N}+1)\Delta x - 2c\Delta t) + \mathcal{O}(\alpha^3). \tag{43}$$

From this result we may solve the equation (42) to give an expression for $W_1(s)$. After some manipulation we have that

$$W_1(s) = -\frac{1}{3\widehat{\varepsilon}}\left((2\mathcal{N}+1)\Delta x + \Delta t\, c\left(\frac{\widehat{\varepsilon} - 3\varepsilon}{\widehat{\varepsilon}}\right)\right) \log\left(\cosh\left(\frac{s}{2\widehat{\varepsilon}}\right)\right) \operatorname{sech}^2\left(\frac{s}{2\widehat{\varepsilon}}\right).$$

We observe from this expression that $W_1(s)$ decays rapidly at infinity, and that the asymptotic ordering of the expression for $W(s)$ is preserved.

A note on the formal error estimates A full rigorous analysis of the validity of the modified equation is not possible using the formal asymptotic methods we have described. However, we will give an estimate of the order of the various errors that arise in this calculation when Δx and Δt are small and of comparable size. The modified equation analysis above has not considered terms of $\mathcal{O}(\Delta x^3)$, $\mathcal{O}(\Delta t^3)$ and $\mathcal{O}(\varepsilon\Delta x^2)$. The first two of these arise principally through the interpolation error estimates, and hence are dominated by terms for the form $\mathcal{O}(\Delta x^3\, V''')$ and $\mathcal{O}(\Delta t^3\, V''')$, which we have shown above to be small. Thus, in the rescaled system, for small α these terms are of order $\mathcal{O}(\alpha^4\Delta x^3)$ etc. In the calculation of the modified diffusion parameter $\widehat{\varepsilon}$ in (39), we must divide this error by $\alpha\Delta t$ and hence, if we assume that Δx and Δt are comparable, the resulting contribution to $\widehat{\varepsilon}$ will then be of order $\mathcal{O}(\alpha\Delta x^2)$. This gives the error term in the expression (4) for $\widehat{\varepsilon}$. Similarly, if we include these extra terms in equation (42) for $\widehat{c}_2$, we divide through by $\alpha^4\Delta t$ to give the error estimate of $\mathcal{O}(\Delta x^2)$, or similar for $\widehat{c}_2$, and hence of $\mathcal{O}(\alpha^2\Delta x^2)$ or similar, for the wave speed $\widehat{c}$. This gives the error term in the expression (5) for $\widehat{c}$.

4. Conclusions from the formal analytical estimates

The analysis in the previous section has predicted the tanh-profile of the travelling wave and the change in the front width and speed. To illustrate these

results we now plot both the effective diffusion parameter $\widehat{\varepsilon}$ and the modified speed $\widehat{c}$ obtained from our analysis in equations (40) and (43) respectively, in the case of a small value of α. For these calculations, as before, we take $c = 1$, $\varepsilon = 10^{-4}$ and the (relatively) small value of $\alpha = 0.1$, and look at the values of $\widehat{\varepsilon}$ and $\widehat{c}$ as functions of $\Delta x = 5/N_x$ for a number of values of $\Delta t = 1.5/N_t$.

4.1. The effective diffusion parameter

The value of the effective diffusion parameter $\widehat{\varepsilon}$ is given in Figure 8, in which we take $10 \leq N_x \leq 1000$ and show results for $N_t = 40, 80$ and 160. In this figure we have also plotted the minimum resolvable diffusion parameter given by ε_{min} in equation (18), visible as the lower bound of the $\widehat{\varepsilon}$ curve. A number
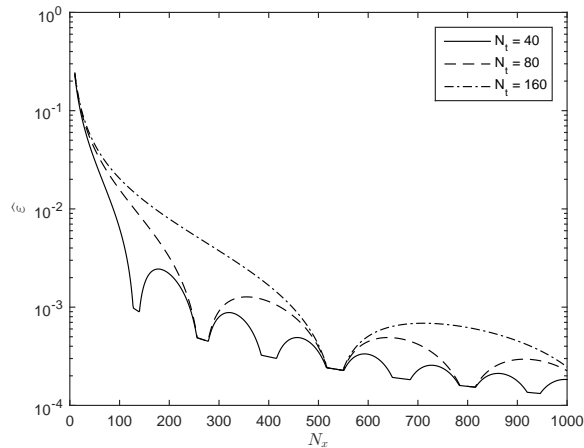
Figure 8: Theoretical estimates for the diffusion parameter $\widehat{\varepsilon}$ including the lower bound of ε_{min}, visible as the lower bound of the $\widehat{\varepsilon}$ curve. In this figure, $\alpha = 0.1$, $N_t = 40$ is given in solid, $N_t = 80$ in dashed and $N_t = 160$ in dashed-dotted. Notice the periodic nature of this graph as the CFL number goes through integer values and the semi-Lagrangian paths cross over the grid points.

of interesting results are apparent from this figure. As expected, the value of $\widehat{\varepsilon}$ overall *decreases* as the value of N_x *increases*. This is useful, and indicates that we will get better front resolution when we have the locally finer meshes used in adaptive methods. However, the effect of the CFL number is also most interesting, and leads to the approximately periodic nature of the graph, caused by the semi-Lagrangian paths crossing over the mesh points. In particular, we see that we can have a *local increase* in $\widehat{\varepsilon}$ as N_x increases as we pass through those values of N_x where the CFL number takes on integer values. A further aspect of the graph is that, for general values of N_x, the value of $\widehat{\varepsilon}$ *increases* when N_t *increases*, and the associated time step Δt *decreases* so that use of *smaller time steps* acts to broaden the front of the solution and thus increase the error in the solution. As reported in Section 2, similar effects have been observed in the application of SISL methods to wave propagation in certain

meteorological problems [McC88]. Furthermore, rigorous results about how the error increases as the time step decreases, when SISL methods are applied to linear advection problems, are given in [FF98].

4.2. The front speed

The effective front speed for the parameters above, given by (43), is plotted as a function of N_x in Figure 9. This figure shows exactly the same qualitative
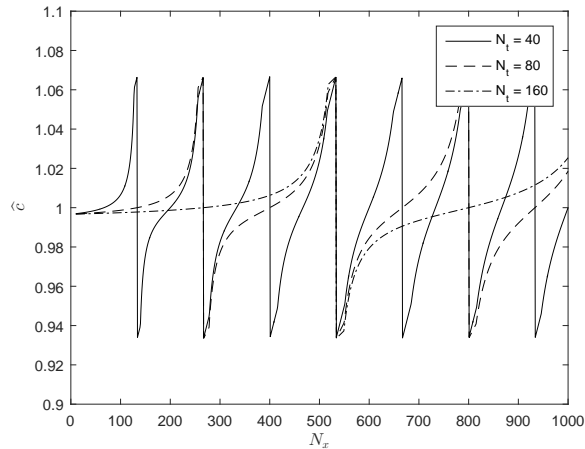
Figure 9: Theoretical estimates for the front speed $\widehat{c}$ as a function of N_x. In this figure, $\alpha = 0.1$, $N_t = 40$ is solid, $N_t = 80$ is dashed and $N_t = 160$ is dot-dashed. Notice again the periodic nature of this graph as the CFL number goes through integer values.

features as the numerically computed results presented in Figure 1.

4.3. The overall error

The overall L_2 error of the solution can be estimated directly from the formula (7). To apply this formula we substitute in the analytic estimates for $\widehat{\varepsilon}$ and $\widehat{c}$ obtained earlier and then integrate over the domain to obtain a semi-analytic estimate for the error. We can see from this figure that the overall error also has a roughly periodic form, oscillating between smaller and larger values as N_x, and in particular the CFL number, varies. The overall error appears to be dominated by the dispersive error, and converges very slowly to zero.

5. Comparisons of the analytical and the numerical error estimates for both linear and higher order interpolation schemes.

5.1. Overview

We now compare the (semi-)analytical estimates of the effective diffusion parameter, the front speed, and the overall error, determined in the previous two
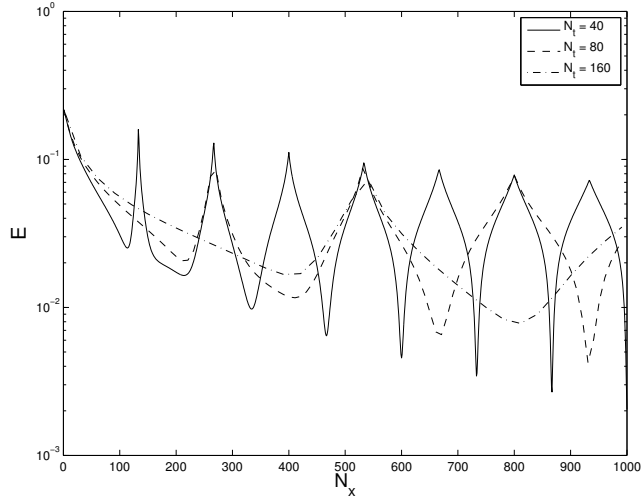
Figure 10: The semi-analytic estimate of the L_2 solution error as a function of N_x and N_t. In this figure, $\alpha = 0.1$. By comparison with Figure 9 we see the dominant effect of the dispersive error, and the periodic nature of this graph as the CFL number goes through integer values.

sections when α is small, with the results of some numerical calculations of the travelling wave solution of Burgers' equation with $\varepsilon = 10^{-4}$, obtained using the SISL method with larger values of α. We also investigate the effect on these estimates of using more general interpolation methods. We consider both the case of small $\alpha = 0.1$ and also the larger value of $\alpha = 0.5$, and take a variety of values of N_x from 10 to 1000 and $N_t = 40, 80, 160$ with, as in Section 4, $\Delta x = 5/N_x$ and $\Delta t = 1.5/N_t$ on an interval $x \in [-1, 4]$. For the first calculations we will consider using linear interpolation, and will then look at numerical results from SISL approximations which use a range of interpolation procedures. In all of our calculations we see, as shown in Section 3, a numerically generated travelling wave solution $U(x, t) = V(x - \widehat{c}\, t)$ of speed $\widehat{c}$ which closely resembles the tanh-profile given in (3). The code was run from $t = 0$ to $t = 1.5$, tracking $x^*(t)$, defined to be the point where $U(x^*(t), t) = c$. The speed $\widehat{c}$ was then calculated as the gradient of the line of best fit, in the least squares sense, for $x^*(t)$. The wave front also has maximum gradient U_x which we can estimate from a finite difference calculation at the mid point of the front and use (17) to obtain the effective diffusion parameter.

5.2. Estimates of the effective diffusion parameter $\widehat{\varepsilon}$

In Figure 11 we show the numerical estimate for the effective diffusion parameter $\widehat{\varepsilon}$ when $\alpha = 0.1$. In this calculation, we combine the estimate (17) for the numerical diffusion with the minimum value estimate ε_{min} given (in the case of linear interpolation) by (18). The curved portion of the graph is the estimate (17), and the more linear portion is the estimate (18). The figure should be compared with Figure 8, and shows very close agreement, both quantitatively

26

and qualitatively, between the numerically calculated and the formal analytic values of $\widehat{\varepsilon}$ for a wide variety of values of N_x and N_t. In particular, Figure 12 shows both the periodic form of $\widehat{\varepsilon}$ predicted as the CFL number changes, and the behaviour that $\widehat{\varepsilon}$ *increases* as Δt *decreases*. This, seemingly counter intuitive behaviour, was first observed [FF98] in applications of the SISL method to linear advection problems in [FF98]. For comparison, in Figure 12 we show both the
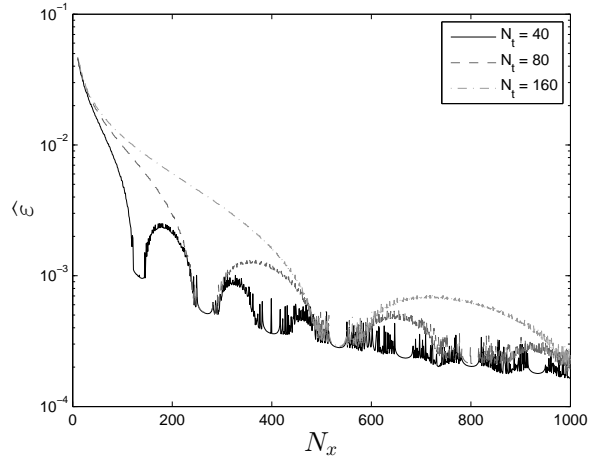
Figure 11: Numerical calculation of the effective diffusion parameter $\widehat{\varepsilon}$ when $\alpha = 0.1$ for various values of N_x and N_t. This figure should be compared with the formal theoretical estimate plotted in Figure 8.

numerical and formal analytic estimates for the modified diffusion parameter $\widehat{\varepsilon}$ when $\alpha = 0.5$. Again we see good agreement, showing that $\widehat{\varepsilon}$ increases as Δt decreases. For larger values of N_x the estimate for the modified diffusion is dominated by the value of ε_{min}, and we do not see all of the finer features of the formula in (4).
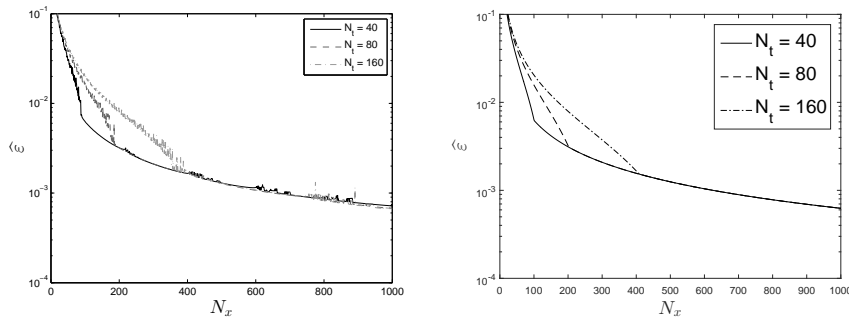
Figure 12: Numerical calculation (left) of the effective diffusion parameter $\widehat{\varepsilon}$ when $\alpha = 0.5$, compared with the formal theoretical estimate (right).

27

5.3. Estimates of the dispersive error

We now examine the dispersive error by comparing the analytic estimates of the modified front speed $\widehat{c}$ with the numerically calculated values. Considering firstly the case of $\alpha = 0.1$, we have already presented the numerically calculated values of $\widehat{c}$ in Figure 1. Comparing the results presented in Figure 1 with the analytic estimates presented in Figure 9, we again see excellent qualitative and quantitative agreement. In particular, we observe that the numerical estimates for $\widehat{c}$ oscillate either side of the true value, with very rapid transitions in the estimate as the CFL number passes through integer values. Furthermore, the deviation of $\widehat{c}$ from the true value of $c = 1$ only decreases very slowly as N_x increases. For comparison we present the results when $\alpha = 0.5$. Figure 13 gives the numerical and theoretical estimates of the front speed, where the analytical estimate obtained taking $\widehat{\varepsilon}$ is taken to be the maximum of the analytical estimate and the minimum estimate $\widehat{\varepsilon} = \alpha \Delta x / 4$. As expected from the larger value of α used, the quantitative agreement between these estimates is worse than for the case of $\alpha = 0.1$. However, there is still some qualitative agreement with, as predicted, the calculated speed oscillating around the true speed as the CFL number increases, with the size of the oscillations only weakly dependent upon N_x.
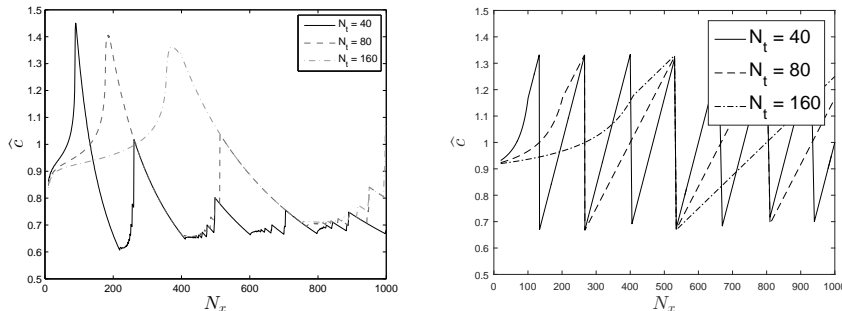
Figure 13: Numerically calculated front speed $\widehat{c}$ (left) for various values of N_t and N_x when $\alpha = 0.5$, compared with the formal theoretical estimate (right).

5.4. Estimates for the overall error

We can also make a direct calculation of the overall L_2 error for the two values of α given. The figure on the left should be compared with the semi-analytic estimate presented in Figure 10 for this value of α and we see good agreement. Observe, as predicted, the super-convergence of the error for certain values of N_x and N_t.

5.5. Numerical results for other interpolation methods and other discretisations

As described in Sections 2 and 3, when SISL methods are used in practice, higher order interpolants, such as a cubic Lagrange, ENO or cubic Hermite function,

28
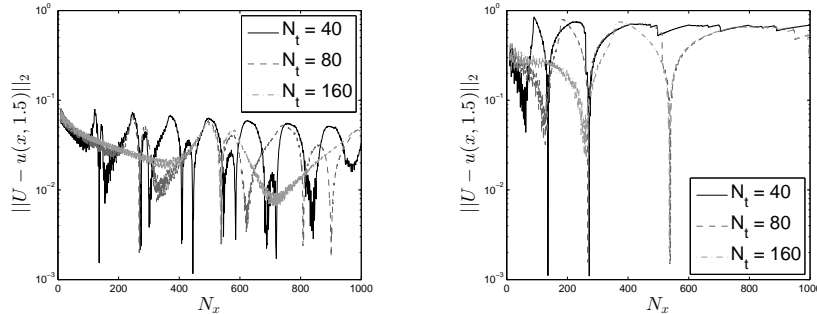
Figure 14: Numerically calculated estimates of the overall L_2 error when $\alpha = 0.1$ (left) and $\alpha = 0.5$ (right).

(both possibly flux limited to reduce oscillations at the front) are usually used. In Figure 6 we saw that when using a monotonic cubic-Hermite interpolant with a flux limiter the numerical solution still has a travelling wave with a tanh-profile with different values if $\widehat{\varepsilon}$ and $\widehat{c}$ from the true solution. In Figure 15 we repeat this calculation using a non monotonic cubic-Hermite interpolation without a flux limiter. As expected this method leads to a solution with more oscillations than those with linear interpolation or with a flux limiter which is an additional error to those so far considered. However, many similar features to the earlier calculations remain. In particular the front has broadened and the front has travelled at a higher speed. Indeed, the dispersive error is dominant. The basic profile of the front can still be represented by a rescaled tanh-profile as before (in this case with $\hat{c} = 1.051$ and $\hat{\varepsilon} = 0.00184$,) with the additional oscillations superimposed on top.

The analysis of the errors in the SISL algorithm with these methods is harder than that presented in Section 3 for the case of linear interpolation with $\theta = 1/2$, but it is straightforward to implement both the higher order interpolation methods and the θ-method with $\theta > 0.5$ numerically. Accordingly we repeat the earlier numerical experiments for Burgers' equation with $\alpha = 0.1$, and calculate the solution U. As we have sees from Figures 6 and 15, it is still appropriate to represent the new solution through a tanh-profile with a modified diffusion parameter $\widehat{\varepsilon}$ and wave speed $\widehat{c}$, and we find these as functions of N_x and N_t using a SISL method with cubic Lagrange, and cubic Hermite [Hym83] interpolation methods [HEOC87], with or without flux limiters [FC80]. One effect of using these higher order interpolants is that the lower bound estimate, found in equation (17) for the linear interpolant, can be reduced when using the higher order interpolant. The results are presented in Figures 16, 18 and 19. Results with an essentially non-oscillatory (ENO) interpolant (not shown) are similar to those with the Hermite interpolant. Comparing these results with those obtained earlier using the linear interpolation method, we see surprisingly little differences to the estimates for $\widehat{\varepsilon}$ and $\widehat{c}$ both qualitatively and quantitatively. In

29
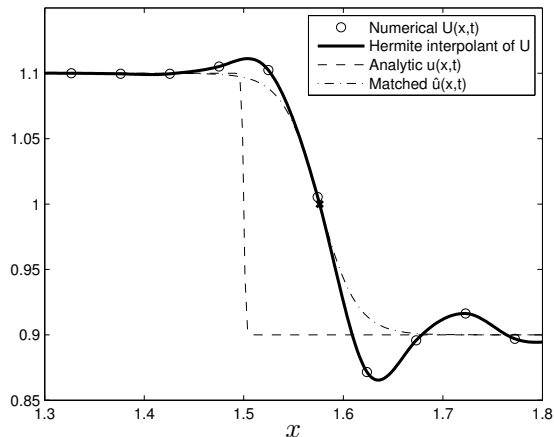
Figure 15: Comparison of the numerical solution with a non monotone cubic-Hermite interpolation scheme U (solid line), with the true solution u (dashed line) and the rescaled tanh-function $\hat{u}(x,t)$ (dash-dot line) at the time $t = 1.5$. In this figure it can be clearly seen that the solution is more oscillatory than before. However the dominant error is dispersive and the front for the numerical solution is ahead of that of the analytical solution as well as being significantly broader. The rescaled tanh-profile $\hat{u}$ is close to point values of the numerical solution with the oscillations imposed on top.

particular, we again see a periodic form to these graphs as the semi-Lagrangian paths cross over the mesh points as the CFL number increases. There is a difference in the effective diffusion parameter, where the minimum estimate due to mesh spacing is lower than in the linear case, because the higher order interpolants can represent sharper fronts, particularly those interpolants without monotonicity enforced. In the latter case this is at the expense of additional oscillations in the solution. The estimate for the speed $\hat{c}$ is very similar in all cases. The overall L_2 error for the cubic-Lagrange method without a limiter is presented in Figure 17. Again this graph is similar to the earlier graph in Figure 10. Although there is an additional oscillatory error due to the approximation of the front, the dominant contribution to the error is dispersive. Again we see certain values of N_x where there is super-convergence.

We also perform experiments with a θ-method with $\theta = 0.55$. In this case the results appeared nearly indistinguishable from the earlier case of $\theta = 0.5$ and are not shown here.

6. Conclusions

In this paper we have presented a modified equation analysis of the diffusive, dispersive and overall L_2 errors which arise when the SISL method is used to approximate a solution to Burgers' equation with a sharp moving front. The modified equation analysis gives a clear picture of the various forms of error

30
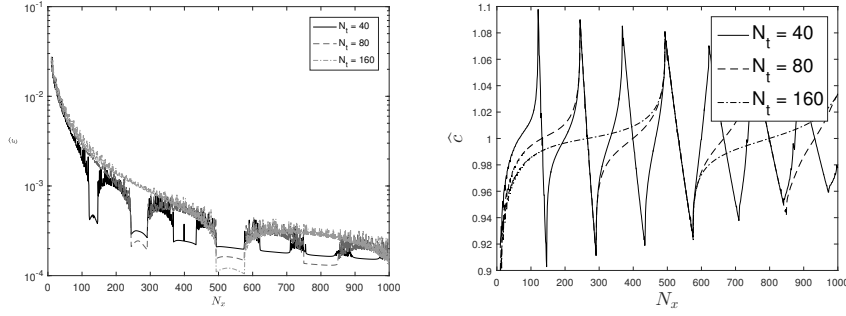
Figure 16: Numerically calculated effective diffusion parameter (left) and front speed (right) for $\alpha = 0.1$, for cubic Lagrangian interpolation with varying N_t and N_x. In this figure the upper estimate for $\widehat{\varepsilon}$ is very similar to that for linear interpolation, but the minimum estimate for $\widehat{\varepsilon}$ is lower.
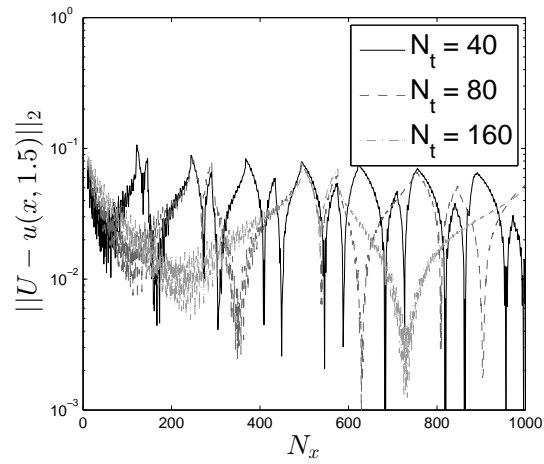
Figure 17: Numerically calculated L_2 solution error with $\alpha = 0.1$, for cubic Lagrangian interpolation with varying N_t and N_x. The dominant contribution to the error in this case remains the dispersive one.

31
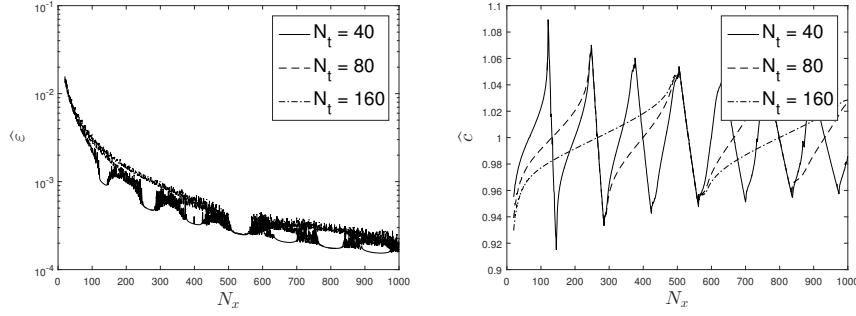
Figure 18: Numerically calculated effective diffusion parameter and front speed for $\alpha = 0.1$, for Hermite interpolation, with Hyman derivative estimates [Hym83] and guaranteed monotonicity [FC80]. In this case the minimum estimate for $\widehat{\varepsilon}$ is closer to that given by the linear interpolant.
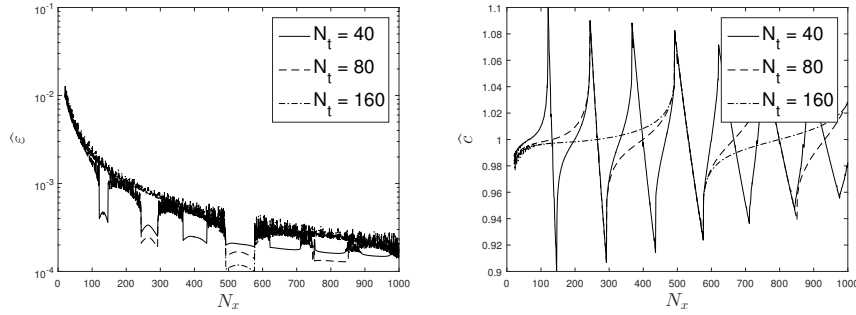
Figure 19: Numerically calculated effective diffusion parameter and front speed for $\alpha = 0.1$, for Hermite interpolation with Hyman derivative estimates [Hym83]. Again we see a lower minimum estimate for $\widehat{\varepsilon}$ but a similar upper estimate to the case of linear interpolation.

that arise when using (monotone) linear interpolation, as well as giving an accurate representation of the solution profile as a rescaled tanh function. The errors computed are largely due to the interpolation error which arises when the departure points are distant from the mesh points. Two conclusions of this analysis and the supporting numerical calculations, are that the front width changes due to the extra diffusion added by this method (in some cases the front width is inversely proportional to the temporal time-step), and that the front speed changes due to a dispersive error. The combined L_2 error shows a combination of these two errors, with the dispersive error dominant, and with super-convergence for certain values of N_x.

Whilst this is to be expected from any discretisation in which the spatial step size Δx is much larger than the correct front width of $\mathcal{O}(\epsilon)$, two remarkable features are evident from this analysis. Firstly, that the front *width* can be well approximated when Δx or Δt are chosen to give an integer value for the CFL number. Secondly that the front *speed* is well approximated at half integer values for the CFL. This leads to the conclusion that if N_x (for example) is chosen carefully for a calculation at two separate values we may be able to resolve the front profile and speed accurately, despite the low resolution of the method, or indeed that there may be values of N_x and N_t giving super-convergent values for the overall L_2 error.

It is also clear from our calculations (and is of course well known), that it is important to use a monotone interpolation scheme to avoid excessive approximation errors.

Finally, the slow convergence of the solution as the spatial step is reduced indicates that it may be inefficient to use a global mesh size reduction in a general calculation. Indeed, as the dominant solution error appears to arise from the interpolation step we are motivated to reduce these errors by using an adaptive mesh method. A combination of a moving mesh strategy with a SISL scheme is the subject of a further paper [CBM19].

Bibliography

[BS92] R. Bermejo and A. Staniforth, *The conversion of semi-Lagrangian advection schemes to quasi-monotone schemes*, Monthly Weather Review **120** (1992), no. 11, 2622–2632.

[CBM19] S. Cook, C. Budd, and T. Melvin, *The moving mesh sisl method*, To appear in J. Comp. Phys. (2019).

[CGM+98] J. Côté, S. Gravel, A. Méthot, A. Patoine, M. Roch, and A. Staniforth, *The operational CMC-MRB Global Environmental Multiscale (GEM) model. part I: Design considerations and formulation*, Monthly Weather Review **126** (1998), 1373–1395.

[CK09] E. Celledoni and B.K. Kometa, *Semi-Lagrangian Runge-Kutta exponential integrators for convection dominated problems*, Journal of Scientific Computing **41** (2009), no. 1, 139–164.

[CXY+08] D. Chen, J. Xue, X. Yang, H. Zhang, X. Shen, J. Hu, Y. Hu, L. Wang, J. LiRen, and J. Chen, *New generation of multi-scale NWP system (GRAPES): general scientific design*, Chinese Science Bulletin **7** (2008), 3433–3445.

[dBS77] C. de Boor and B. Swartz, *Piecewise monotone interpolation*, Journal of Approximation Theory **21** (1977), no. 4, 411–416.

[Dre83] L. Dresner, *Similarity solutions of nonlinear partial differential equations*, Pitman, London, 1983.

[FC80] F.N. Fritsch and R.E. Carlson, *Monotone piecewise cubic interpolation*, SIAM Journal on Numerical Analysis **17** (1980), no. 2, 238–246.

[FF98] M. Falcone and R. Ferretti, *Convergence analysis for a class of high-order semi-lagrangian advection schemes*, SIAM Journal on Numerical Analysis **35** (1998), 909–940.

[GNQ14] Wei Guo, R.D. Nair, and Jing-Mei Qiu, *A conservative semi-lagrangian discontinuous galerkin scheme on the cubed sphere*, Monthly Weather Review **142** (2014), no. 1, 457–475.

[GPF03] F.X. Giraldo, J.B. Perot, and P.R. Fischer, *A spectral element semi-lagrangian (sesl) method for the spherical shallow water equations*, Journal of Computational Physics **190** (2003), 623–650.

[HEOC87] A. Harten, B. Engquist, S. Osher, and S.R. Chakravarthy, *Uniformly high order accurate essentially non-oscillatory schemes, III*, Journal of Computational Physics **71** (1987), no. 2, 231–303.

[HLW06] E. Hairer, C. Lubich, and G. Wanner, *Geometric numerical integration: Structure-preserving algorithms for ordinary differential equations*, Springer, 2006.

[Hym83] J.M. Hyman, *Accurate monotonicity preserving cubic interpolation*, SIAM Journal on Scientific and Statistical Computing **4** (1983), no. 4, 645–654.

[KW90] Hung-Chi Kuo and R.T. Williams, *Semi-Lagrangian solutions to the inviscid Burgers equation*, Monthly Weather Review **118** (1990), no. 6, 1278–1288.

[LeV02] R.J. LeVeque, *Finite volume methods for hyperbolic problems*, vol. 31, Cambridge University Press, 2002.

[LOC94] Xu-Dong Liu, S. Osher, and T. Chan, *Weighted essentially non-oscillatory schemes*, Journal of computational physics **115** (1994), no. 1, 200–212.

[LR05] B. Leimkuhler and S. Reich, *Simulating hamiltonian dynamics*, Cambridge University Press, 2005.

[McC88] J.D. McCalpin, *A quantitative analysis of the dissipation inherent in semi-Lagrangian advection*, Monthly Weather Review **116** (1988), no. 11, 2330–2336.

[McD84] A. McDonald, *Accuracy of multiply-upstream, semi-Lagrangian advective schemes*, Monthly Weather Review **112** (1984), no. 6, 1267–1275.

[McD87] _____, *Accuracy of multiply-upstream semi-Lagrangian advective schemes II*, Monthly Weather Review **115** (1987), no. 7, 1446–1450.

[MM94] K.W. Morton and D.F. Mayers, *Numerical solutions of partial differential equations: An introduction*, Cambridge University Press, 1994.

[Pow81] M.J.D. Powell, *Approximation theory and methods*, Cambridge University Press, 1981.

[Rob81] A. Robert, *A stable numerical integration scheme for the primitive meteorological equations*, Atmos.-Ocean **19** (1981), 35–46.

[Rob82] _____, *A semi-Lagrangian and semi-implicit numerical integration scheme for the primitive meteorological equations*, Japan Meteor. Soc. **60** (1982), 319–325.

[RTS+95] H. Ritchie, C. Temperton, A. Simmons, M. Hortal, T. Davies, D. Dent, and M. Hamrud, *Implementation of the semi-Lagrangian method in a high resolution version of the ECMWF forecast model*, Monthly Weather Review **123** (1995), 489–514.

[RW90] P.J. Rasch and D.L. Williamson, *On shape-preserving interpolation and semi-Lagrangian transport*, SIAM Journal on Scientific and Statistical Computing **11** (1990), no. 4, 656–687.

[SC91] A. Staniforth and J. Côté, *Semi-lagrangian integration schemes for atmospheric models - a review*, Monthly Weather Review **119** (1991), no. 9, 2206–2223.

35

[Smi00] C.J. Smith, *The semi-lagrangian method in atmospheric modelling*, Ph.D. thesis, University of Reading, 2000.

[TB15] G. Tumolo and L. Bonaventura, *A semi-implicit, semi-lagrangian discontinuous galerkin framework for adaptive numerical weather prediction*, Quarterly Journal of the Royal Meteorological Society **141** (2015), 2582–2601.

[THA01] C. Temperton, M. Hortal, and Simmons A.J., *A two-time-level semi-Lagrangian global spectral model*, Quarterly Journal of the Royal Meteorological Society **127** (2001), 111–126.

[TX07] Tao Tang and Jinchao Xu (eds.), *Adaptive computations: Theory and algorithms*, Mathematics Monograph Series 6, Science Press, 2007.

[WSW+14] N. Wood, A. Staniforth, A. White, T. Allen, M. Diamantakis, M. Gross, T. Melvin, C. Smith, S. Vosper, M. Zerroukat, et al., *An inherently mass-conserving semi-implicit semi-lagrangian discretization of the deep-atmosphere global non-hydrostatic equations*, Quarterly Journal of the Royal Meteorological Society **140** (2014), no. 682, 1505–1520.